VIA MEDICA

Nuclear Medicine Review 2019, 22, 2: 45–55
DOI: 10.5603/NMR.a2019.0016

ISSN 1506–9680

Original

Evaluation the effect of different collimators and energy window on Y-90 bremsstrahlung SPECT imaging by SIMIND Monte Carlo program

Nazila Shahmari, Payvand Taherparvar
Department of Physics, Faculty of Science, University of Guilan, Rasht, Iran

[Received 10 VI 2018; Accepted 11 VI 2019]
Compliance with Ethical Standards:
Conflict of Interest: The authors declare that there are no conflicts of interest in connection with this paper.
Ethical approval: This article does not contain any studies with human participants or animals performed by any of the authors.

Abstract

BACKGROUND: Recently, the treatment efficiency of Yttrium 90 (Y-90) and providing reliable estimates of activity by single photon emission computed tomography (SPECT) imaging of bremsstrahlung radiation released during beta therapy have been evaluated. In the Y-90 bremsstrahlung SPECT imaging, the resulting energy spectrum is very complex and continuous, which creates many difficulties in the imaging protocol and image reconstruction. Furthermore, image quality and quantitative accuracy in the bremsstrahlung SPECT imaging are affected by collimator penetration and scatter. So, the collimator type and its geometry have impressive effects on the spatial resolution, system sensitivity and image contrast.
MATERIAL AND METHODS: Hereby, in this paper, we evaluated the effect of the energy window (three energy windows: 60 to 160 keV, 160 to 400 keV, and 60 to 400 keV) and the commercial parallel-hole collimators with different geometric parameters on the Y-90 bremsstrahlung spectrum and the image quality of the liver tumors based on criteria such as system sensitivity and image contrast. SIMIND Monte Carlo simulation code was used to generate the Y-90 bremsstrahlung SPECT images of the liver tumor with different diameters: 1.36, 2.04, 2.72, 3.4, 4.08, and 4.76 cm by use of the digital Zubal phantom. Furthermore, the tumor size was estimated by evaluating pixel intensity profile on the line drawn through the activity distribution image.
RESULTS: Our results showed that the collimator choice and energy window setting in the bremsstrahlung SPECT imaging have significant effects on the image quality and tumor size estimation. Optimal image quality could be acquired by the energy window of 60 to 400 keV and the SPECT system equipped with a Medium-Energy General-Purpose (MEGP) collimator of Millennium VG Kameran (GV) Company. Moreover, the estimation of distribution size was close to the actual value for tumor sizes larger than 2.04 cm, especially by using the SPECT system equipped with the GV-MEGP collimator in the wide energy window.
CONCLUSIONS: We found an optimal collimator to be more appropriate for improving the imaging quality of Y-90 bremsstrahlung photons, which can be used for reliable activity distribution estimates after radiation therapy.

KEY words: Yttrium-90, SPECT, energy window, parallel-hole collimators, image contrast, bremsstrahlung, Monte Carlo simulation

Nucl Med Rev 2019; 22, 2: 45–55

Introduction

Treatment with yttrium-90 (^{90}Y) microspheres is a minimally invasive technique that combines embolization and radiation therapy to treat liver cancer. This radionuclide emits short-ranged beta radiation with a physical half-life of 64.1 hours (2.67 days). The emitted photons have a maximum energy of 2.3 MeV, with an average energy of 0.93 MeV, and mean and maximum penetration range of 2.5 mm and 11 mm in soft tissue, respectively [1]. Y-90 has been widely used in targeted radionuclide therapy (TRT), because of sufficient energy of β-particles emitted during its decay and a proper half-life. This radionuclide is used for the treatment of primary and metastatic liver cancers, via microsphere radioembolization, and

Correspondence to: Assistant Professor Payvand Taherparvar
Faculty of Science, Department of Physics, Namjoo Avenue, University of Guilan, P.O. Box 41635-1914, Rasht, Guilan, Iran;
e-mail: p.taherparvar@guilan.ac.ir; p.taherparvar@gmail.com

lymphatic system cancers such as non-Hodgkin's lymphoma [2]. Recently, radiation therapy treatment efficiency has been evaluated using the Y-90 bremsstrahlung single photon emission computed tomography (SPECT) imaging that shows the distribution of the radionuclide within the patient's body [3]. In the Y-90 SPECT imaging, most of the Y-90 bremsstrahlung photons are created from the interaction of β-particles with the patient's tissues. Due to the fact that bremsstrahlung photons have a continuous and broad energy spectrum, unlike the conventional radioisotopes used for diagnostic imaging, Y-90 SPECT images usually have poor quality including low contrast [2, 4]. Scattered photons and septal penetration events also lead to a decrease in the Y-90 bremsstrahlung SPECT image quality, which is influenced by acquisition parameters (such as energy window and collimator) [2]. High-Energy (HE) or Medium-Energy (ME) parallel-hole collimators, which are particularly designed for radionuclides such as gallium-67 (Ga-67) or iodine-131 (I-131) [2, 5], are used in order to minimize septal penetration of the high-energy bremsstrahlung photons. The collimator, which is a critical factor in the SPECT imaging system, is used to collimate radiation from source and absorb secondary radiation scattered by an object.

The absorption of incident photons by collimator decreases the system sensitivity and improves spatial resolution [6]. Therefore, the choice of the appropriate collimator is one of the most important factors to acquire high quality SPECT images. Unfortunately, high sensitivity, high resolution, and small fraction of septal penetration and scatter are usually mutually exclusive factors in the collimator design [2]. Indeed, there is a trade-off between sensitivity and spatial resolution, which is determined by choice of collimator configuration [7]. The performance of parallel-hole collimator is influenced by its geometry (i.e. hole length, hole diameter, and septal thickness) [7] which has direct effects on the image quality, system sensitivity, and activity distribution assessment in the Y-90 bremsstrahlung SPECT imaging [8]. On the other hand, the better size estimation of liver tumor is helpful as a prognostic indicator during the treatment [9]. One of the methods to determine tumor size in the nuclear medicine imaging is based on the evaluation of pixel intensity profile on the line drawn through the activity distribution image, which is often Gaussian distribution function. The size of the tumor is determined by measuring the full width at half maximum (FWHM) of the intensity profile of pixels. Since spatial resolution and system sensitivity are affected by the collimator hole length and diameter, the estimation of tumor size will be affected by the collimator characteristics.

Some studies have been done to optimize the energy window and collimator for quantitative and qualitative Y-90 bremsstrahlung SPECT imaging. Roshan et al. studied the effect of the hole diameter of the special parallel-hole collimator with fixed collimator and septal thickness values on the image contrast to improve the image quality of Y-90 bremsstrahlung SPECT images [7]. Rong et al. have developed a new method to optimize the energy windows in quantitative imaging of Y-90 bremsstrahlung SPECT when bias is a vital factor limiting reliability [10]. Roshan et al. also provided a review of the methods of energy window, collimator and reconstruction algorithm optimizing for Y-90 bremsstrahlung SPECT imaging to improve the treatment efficacy of liver tumor radioembolization using Y-90 microspheres [11]. Walrand et al. evaluated the optimal design of an Anger camera–collimator system for Y-90 bremsstrahlung SPECT imaging by Monte Carlo simulations [8]. Also, other studies have been done to optimize the collimator for evaluating quantitative Y-90 bremsstrahlung SPECT imaging [2, 3]. But until now, the effect of the most common parallel-hole collimators available in the clinical centers has never been studied for bremsstrahlung SPECT imaging.

Furthermore, studies have shown that the estimation of tumor size is useful in the assessment of liver tumor response to therapy, especially in the early stage of treatment [12]. The activity distribution in post-radioembolization SPECT images shows the distribution of the injected Y-90 microspheres, which accumulate mainly in the tumor. Then, the estimation of tumor size, which is helpful in evaluating the response to therapy, can be performed by using distribution of the injected microspheres, although in a few cases the activity distribution in post-radioembolization SPECT images may not correspond to the actual tumor location. Numbers of studies have been done to predict the tumor size in the nuclear medicine images by using FWHM method [13, 14]. But until now, the effect of the energy window width and collimator on the estimation of the liver tumor size has never been studied for Y-90 bremsstrahlung SPECT imaging. Due to the low image quality of Y-90 bremsstrahlung SPECT images, it is necessary to improve the estimation ability of the injected microspheres distribution size by selecting the proper imaging protocol.

In this paper, we studied the effect of different geometries of standard parallel-hole collimators (such as hole diameter, hole shape, hole length, and collimator thickness) based on the characteristics of the most common collimators on the Y-90 SPECT image quality of the liver tumors with different sizes in the three energy windows. Furthermore, the estimation of tumor size was performed by images acquired with different collimators. We used SIMIND Monte Carlo (MC) simulation code and Zubal phantom to generate the Y-90 bremsstrahlung SPECT images of the liver tumors with different sizes. The image contrast and the estimation of tumor size were utilized to compare the images acquired with different collimators. This study was done to identify the best collimator and energy window for the better acquisition of Y-90 bremsstrahlung SPECT images.

Materials and methods

Monte Carlo simulation

In this study, Y-90 bremsstrahlung images were generated using the simulated Siemens E.CAM SPECT system by the SIMIND Monte Carlo code version 6.0 [15]. The validation of the SIMIND for Y-90 bremsstrahlung imaging was done according to the previous studies [4, 7].

We used the digital Zubal phantom (developed by George Zubal) with uniform activity distribution within the liver together with a hot tumor. The Zubal phantom is a digital representation of an adult male obtained from a CT scan. The data has been segmented into about 50 different tissue types. The original dataset consists of 243 × 128 × 128 voxels, with 8-bit depth. Each tissue type is represented by an arbitrary integer [16]. Tumors were positioned at the center of the liver tissue. The cumulative treatment activity of the Y-90 microspheres was chosen 1.5 GBq with the tumor-to-liver activity concentration ratio of 10:1, which were selected based on the previous studies [4, 10]. It was assumed

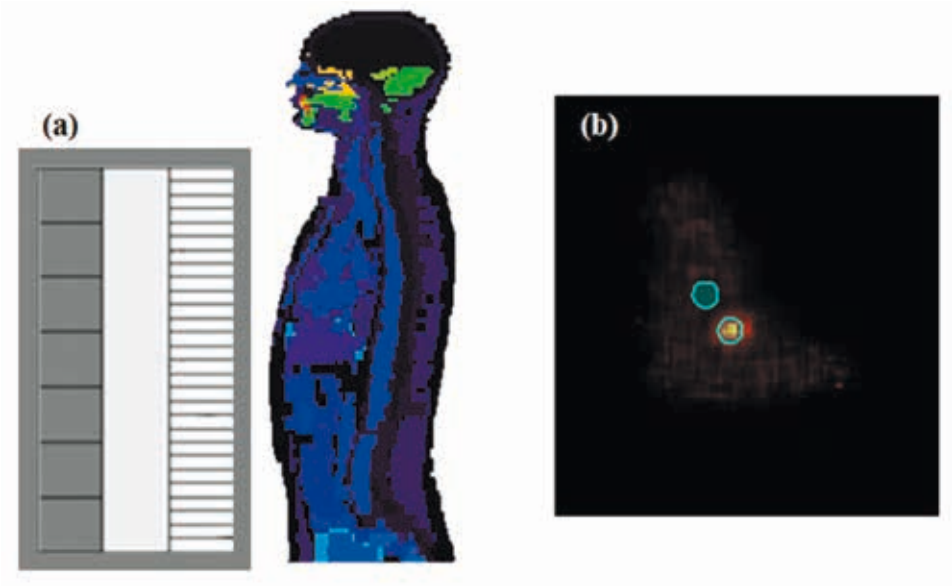

Figure 1. (A) Sagittal Section of the Zubal phantom and gamma camera. **(B)** Reconstructed image of the liver tumor, along with two ROIs: ROIs belonging to the tumor and background

there was no activity outside the liver, a reasonable assumption for microsphere brachytherapy. The digital Zubal phantom including liver tumor was aligned lengthwise along the scanner axis and centered, as shown in Figure 1A. The phantom surface to the collimator lower surface was adjusted 25 cm. We simulated tumors of different diameters: 1.36, 2.04, 2.72, 3.4, 4.08, and 4.76 cm with the same activity concentration to evaluate the image contrast in each step. Separate SPECT images were acquired for each of the tumors in step and shoot mode, with 128 projections, matrices of 128 × 128 pixels with a pixel size of 0.34 cm, 360° counter-clockwise rotation in SPECT, 1.5 million counts per projection, and the imaging time of 30 s per projection view.

Scattered radiation and photons penetration through the collimator septal are the image-degrading effects in the Y-90 bremsstrahlung SPECT imaging. In the image reconstruction of Y-90 SPECT imaging, it is necessary to correct the effects of attenuation for imaging. A method for determining the attenuation map is using CT scan and entering the effects of attenuation coefficient in reconstruction process. Generally in this case, the iterative algorithms are used for image reconstruction [4]. In our study, the projections were reconstructed using an Ordered Subsets Expectation Maximization (OS-EM) reconstruction algorithm with 150 iterations and 16 subsets including compensations for attenuation and collimator response using MATLAB 2013a [17]. Correction for photon attenuation within the phantom was made with an attenuation map created by the Zubal phantom.

Rong and Frey believed that the optimal geometric resolutions of a hexagonal-hole collimator (R) for Y-90 bremsstrahlung imaging should be between 1 and 1.8 cm [2]. Because higher values of R would not be desirable due to the large bias in the activity estimates, and lower values of R lead to the large variance of the activity estimates, hence would not be desirable [2]. The geometric resolution depends on the hole length (H), hole diameter (D), and septal thickness (T). Thus, in order to improve the image quality in the Y-90 bremsstrahlung SPECT imaging, we studied the effect of different conventional collimators with different resolution and sensitivity (according to hole diameter and shape, septal thickness, and collimator thickness) on the image quality of Y-90 bremsstrahlung SPECT images. The geometric resolutions of these collimators are between 1 and 2.3 cm for a Y-90 point source located at a distance of 15 cm from the collimator surface. Since the collimator geometric parameters (septal thickness, collimator thickness, and hole diameter) can be changed individually in the SIMIND code, we used geometric parameters of commercial collimators available for SPECT imaging. We used geometric parameters of Medium-Energy (ME) and High-Energy (HE) parallel-hole collimators of different companies, as listed in Table 1, including GE (General Electric),

Table 1. Geometric parameters of ME and HE parallel-hole collimators available for SPECT imaging

Collimator	Septal thickness [cm]	Collimator thickness [cm]	Hole diameter [cm]
AD-HEGP	0.1727	6	0.381
AD-MEGP	0.1143	4.8	0.295
GE-HEGP	0.32	4	0.4
GE-MEGP	0.14	4.2	0.34
GV-HEGP	0.18	6.6	0.4
GV-MEGP	0.105	5.8	0.3
ME-HEGP	0.16	5.5	0.34
ME-MEGP	0.12	3.5	0.25
PB-HEGP	0.173	5.84	0.381
PB-MEGP	0.086	5.84	0.34
SE-HE	0.2	5.08	0.34
SE-ME	0.114	4.064	0.294
SY-HE	0.2	5.97	0.4
PX-MEGP	0.086	5.840	0.470
NU-HEGP	0.025	2.540	0.203
SI-ME+*	0.066	3.284	0.207

*ME+: Medium Energy Parallel E.CAM+

GV (Millennium VG Kameran), PB (Philips Brightview Camera), ME (Mediso Nucline Spirit DH-V), SE (E.CAM Siemens Medical System), PX (Picker System AXIS/IRIX System), NU (Nuclear Technologies Hexarray), AD (Adac Vertex System), SY (Siemens Medical System Symbia Collimators), and SI (Siemens Medical System). The collimators with similar characteristics were excluded.

In the energy spectrum of the Y-90 bremsstrahlung photons, most photons with energies lower than 60 keV are attenuated in the patient body. Furthermore, the large numbers of photons with energies higher than 500 keV can penetrate in the collimator septal [15]. Thus, we studied the three energy windows including energy windows ranging from 60 to 160 keV, 160 to 400 keV, and 60 to 400 keV to generate the optimal energy window for different collimators.

Evaluation of the image quality

We calculated the image contrast to evaluate the quality of the reconstructed Y-90 SPECT images. Image contrast was calculated for the hot tumor (with the various diameters from 1.36 to 4.76 cm) of the liver using equation (1):

$$C_l = (R_l - R_o)/R_o \quad (1)$$

where R_l is the mean pixel values of the activity of hot tumor and R_o is the mean pixel values of the background activity (the liver tissue). To measure R_l a circular region of interest (ROI) was placed over the tumor on the reconstructed image. The ROI size was set according to the size of simulated tumor. To measure R_o an arbitrary ROI excluding the ROI belonging to the hot tumor was used in the liver tissue on the reconstructed image, which its size was chosen similar to the tumor size for each simulated tumor, as shown in Figure 1B.

We studied the FWHM of the intensity profile of pixels to estimate the size of each simulated spherical liver tumor. The intensity distribution was fitted by a Gaussian function and its FWHM was calculated to estimate the size of the tumor. We calculated the tumor size using FWHMx3.4 equation, where 3.4 is the pixel size in mm. Then, the measured size of the microsphere distribution was compared with true tumor size. This process was performed for each of the tumors with the different size, separately.

Results

In this paper, we assessed the effect of the conventional parallel-hole collimators, which have the geometric resolutions between 1 and 2.3 cm, and the energy window; including three energy windows ranging from 60 to 160 keV (the1st energy window), 160 to 400 keV (the 2nd energy window), and 60 to 400 keV (the 3rd energy window) on the Y-90 bremsstrahlung energy spectrum and the contrast of reconstructed images of the liver tumor with the different size. The Zubal anthropomorphic whole body phantom consists of a liver tumor with six different diameters ranging from 1.36 to 4.76 cm was used to simulate the distribution of Y-90 in the patient body.

Figure 2 shows the effect of different collimators with different geometric parameters (Tab. 1) on the Y-90 bremsstrahlung energy spectrum for the tumor size of 3.4 cm, which was generated by simulation of the SPECT system equipped with the 16 collimators using the SIMIND Monte Carlo code. As can be seen in the Figure 2, the numbers of the detected bremsstrahlung photons (counts) on the whole range of the energy spectrum are different for the various collimators. The NU-HEGP collimator has the maximum count statistics in comparison to the others, which is due to the smaller septal thickness, as seen in Table 1, which permits more septal penetration than the other collimators. There are similar conditions for other tumor sizes, to some extent.

Diagrams in Figure 3 show the effect of energy window and selected collimators on the image contrast of Y-90 bremsstrahlung SPECT images of tumors with the various diameters, which were located deep inside the liver tissue. The results show that the best contrast for the tumor images was achieved by use of the energy window width of 60–400 keV. Moreover, the image contrast using an energy window width of 60–160 keV was better than the

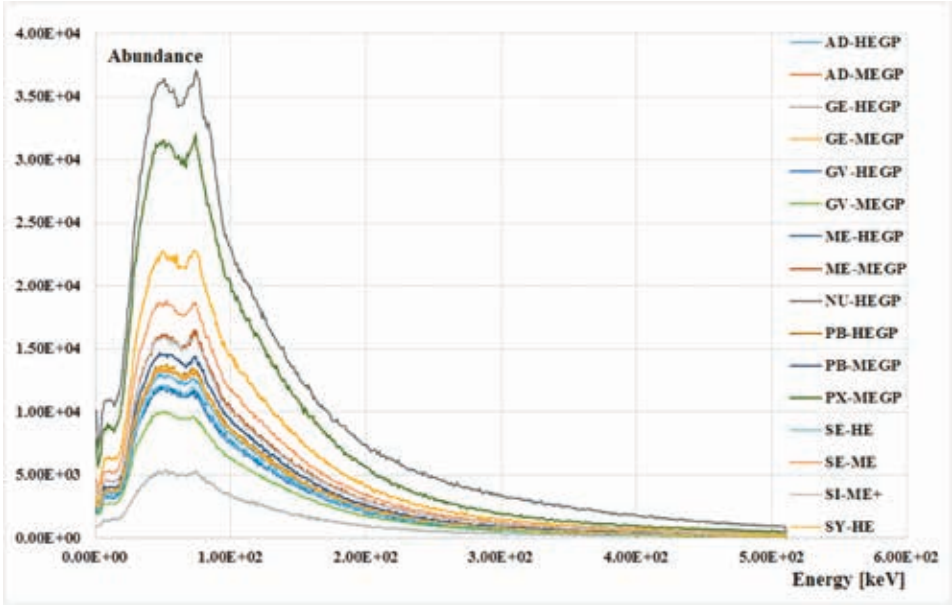

Figure 2. Energy spectrum of Y-90 bremsstrahlung photons which was generated by use of the SIMIND simulation of a SPECT system equipped with different collimators

Figure 3. The image contrast of the liver tumor [with different diameters: 1.36 **(A)**, 2.04 **(B)**, 2.72 **(C)**, 3.4 **(D)**, 4.08 **(E)**, and 4.76 cm **(F)**] for SPECT imaging with the various collimators in the three energy windows: 60–160 keV, 160–400 keV and 60–400 keV

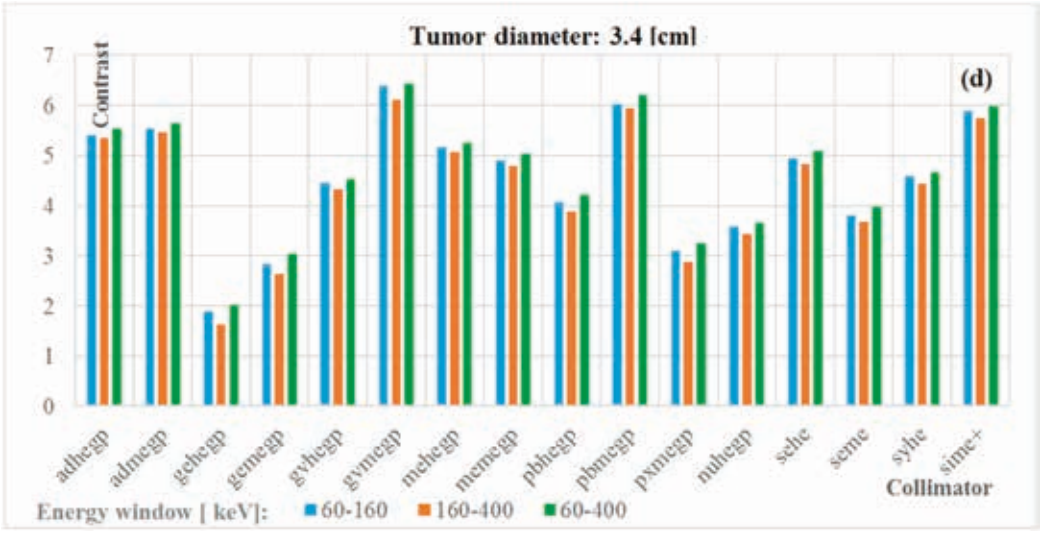

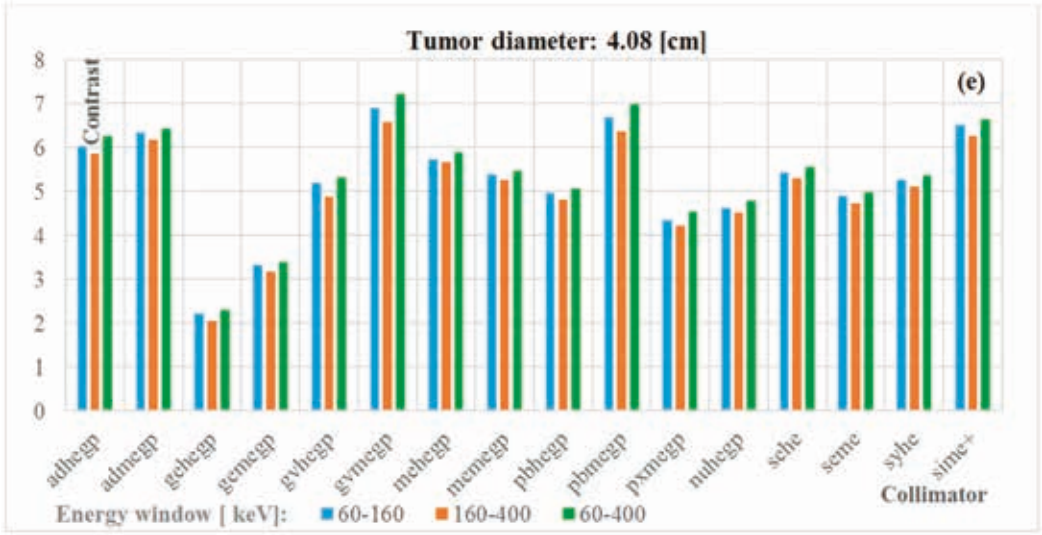

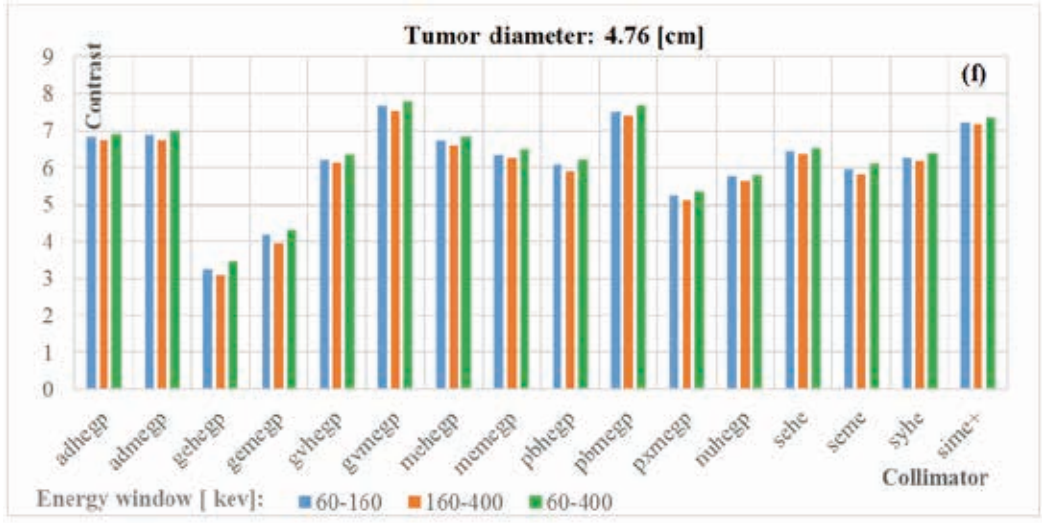

Figure 3. cd. The image contrast of the liver tumor [with different diameters: 1.36 **(A)**, 2.04 **(B)**, 2.72 **(C)**, 3.4 **(D)**, 4.08 **(E)**, and 4.76 cm **(F)**] for SPECT imaging with the various collimators in the three energy windows: 60–160 keV, 160–400 keV and 60–400 keV

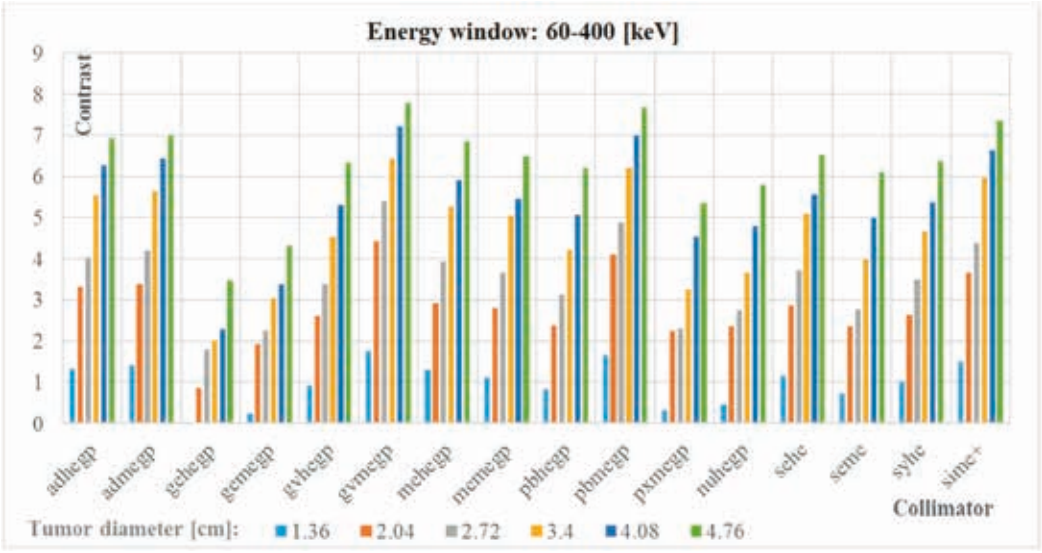

Figure 4. The image contrast of the liver tumor (with different diameters) for SPECT imaging with the various collimators in the best energy window: 60–400 keV

energy window width of 160–400 keV. On the other hand, the Medium-Energy General-Purpose (MEGP) collimator of Millennium VG Kameran (GV) Company showed better image contrast in comparison to the other parallel-hole collimators in the three energy windows and the High-Energy General-Purpose (HEGP) collimator of General Electric (GE) company decreased the image contrast of Y-90 SPECT imaging. Totally, the ME collimators have the potential to improve the image contrast of Y-90 bremsstrahlung images, although in few cases the HE collimators could provide better results than ME collimators.

Comparison of the contrast diagrams for different collimators in Figure 3 indicates that with increasing tumor size, the tumor image contrast was also increased in each of three energy windows. The results show that the maximum value of the contrast was obtained by use of the GV-MEGP collimator for the tumor size of 4.76 cm in the wide energy window (60–400 keV). Figure 4 shows the results of the image contrast of the liver tumors in the best energy window (60–400 keV). As shown in the figure, the image contrast was improved with increasing tumor size, and the image contrast values were highest for the GV-MEGP collimator. Furthermore, the worst results belonged to the SPECT data acquisition with the GE-HEGP collimator, as the tumor size of 1.36 cm was not detectable by the SPECT system equipped with this collimator. Hereby, we did not calculate its image contrast in Figure 3A.

Table 2 shows the fractions of penetrating and scattered photons that contribute to images generated by the SIMIND code for different collimators. Moreover, the results of the sensitivity of the SPECT system with the various collimators are presented in the table. We can see that the scatter fraction results are similar to each other, while the NU-HEGP collimator provided the highest septal penetration fraction in comparison with the other collimators, which is due to the smaller septal thickness than the others. The results show that the best sensitivity was also acquired with this collimator, which is consistent with the results in Figure 2. Because the NU-HEGP collimator does not have the largest hole diameter, increasing the system sensitivity by using this collimator is due to the smaller septal thickness and highest level of septal penetration. On the other hand, a small fraction of the septal penetration was found for the GE-HEGP collimator due to the greater septal thickness.

Table 2. Fraction of penetration and scatter, as well as system sensitivity for the sixteen collimators, which were generated by the SIMIND code

Collimator	Penetration [%]	Scatter [%]	Sensitivity [cps/MBq]
AD-HEGP	0.73	0.64	4.5155
AD-MEGP	0.94	0.70	4.6787
GE-HEGP	0.79	0.80	1.8166
GE-MEGP	1.01	0.70	7.8823
GV-HEGP	0.62	0.55	4.1167
GV-MEGP	0.81	0.65	3.4824
ME-HEGP	0.75	0.61	4.2068
ME-MEGP	1.15	0.71	5.6561
NU-HEGP	1.37	0.52	12.6813
PB-HEGP	0.66	0.57	4.7648
PB-MEGP	0.71	0.60	5.1275
PX-MEGP	0.73	0.59	10.9396
SE-HE	0.81	0.62	4.2208
SE-ME	0.97	0.65	6.5584
SI-ME+	1.13	0.64	5.5887
SY-HE	0.75	0.63	4.7248

A visual comparison between the tumor (2.04 cm) SPECT images in the two energy windows (60–400 keV and 160–400 keV), as shown in Figure 5A, demonstrates that bremsstrahlung SPECT imaging with the GV-MEGP collimator could produce the optimal image quality and better recognition of the liver tumor in the wide energy window.

Visual comparison of adjacent images in Figure 5A shows that the wide energy window also provided the optimal image quality for the various collimators. Further, comparison between the first

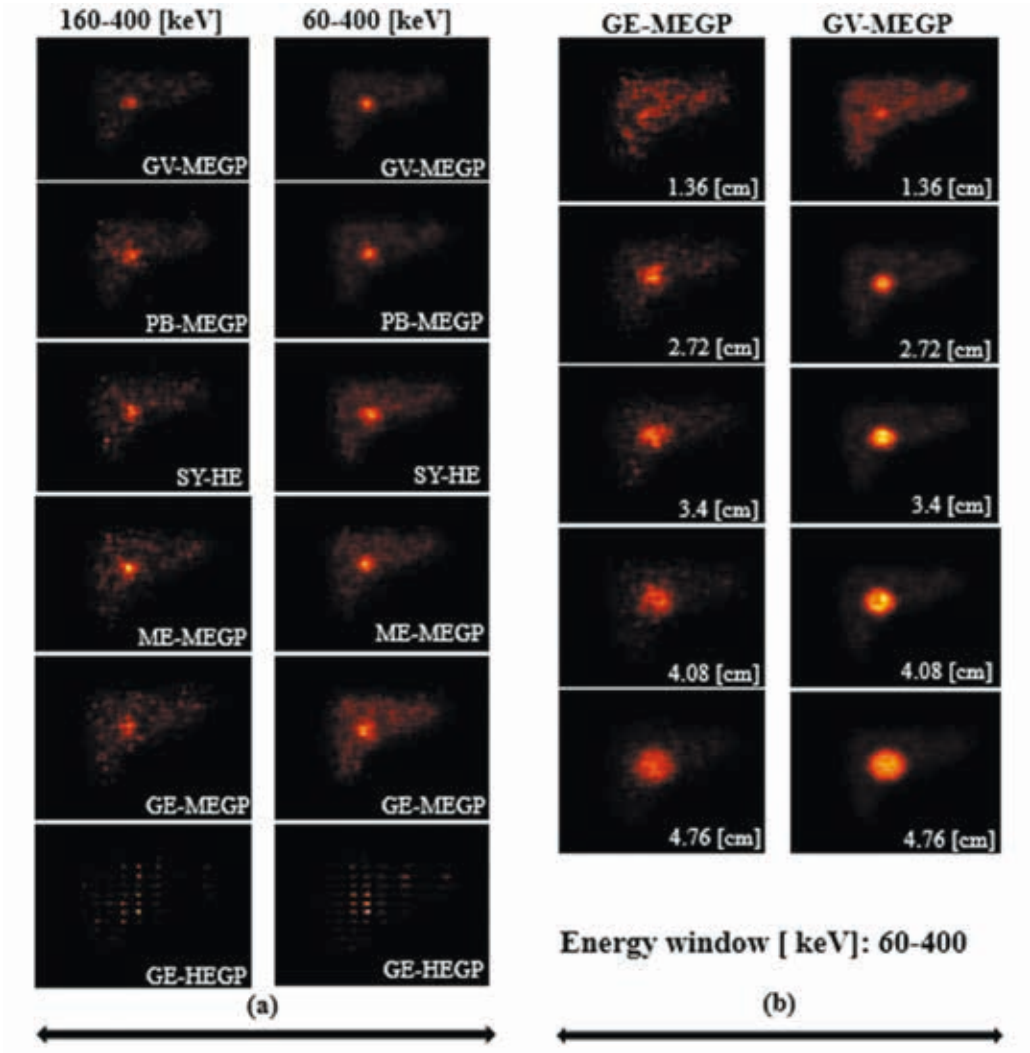

Figure 5. (A) Reconstructed images of the liver tumor (2.04 cm) which were generated by use of the various collimators in the two energy windows: 160–400 keV and 60–400 keV. **(B)** Reconstructed images of hot liver tumor with different diameters: 1.36, 2.72, 3.4, 4.08, and 4.76 cm which were obtained by use of the GV-MEGP and GE-MEGP collimators

column images and the second column images in Figure 5A shows that the tumor image quality could be improved by use of the GV-MEGP collimator in different energy windows. Figure 5B shows the reconstructed liver tumor images in the best energy window (60–400 keV) for the two collimators including the GV-MEGP collimator, which produced the best results, and the GE-MEGP collimator, which produced a poor quality of Y-90 bremsstrahlung SPECT images. The superiority of the GV-MEGP collimator is still observed, especially in the wide energy window for all sizes of tumors.

The size of distribution in the Y-90 SPECT imaging, which can estimate the tumor size, has been calculated by evaluation of the pixel intensity profile on the line drawn through the tumor image and calculating its FWHM. This procedure was done for all of the SPECT images, which were acquired by simulation of the SPECT system equipped with the various collimators in the three energy windows. Figure 6 shows the relationship between the actual liver tumor sizes (diameters) and the estimated sizes in the different acquisition energy windows for the three collimators which produced the better results in terms of the image contrast including GV-MEGP, PB-MEGP, and SI-ME+ collimators.

The results indicate that the estimation of tumor sizes is close to the actual values, to some extent, by use of the wide energy window and the GV-MEGP collimator for the tumor sizes larger than 2.04 cm. Differences between actual and estimated dimensions of the liver tumors were increased as the dimensions of the liver tumor decreased particularly for the tumor size smaller than 2.04 cm.

Discussion

The simulations of the Y-90 bremsstrahlung SPECT images were performed for different sizes of the liver tumor using different collimators in the three energy windows: 60–160 keV, 160–400 keV, and 60–400 keV. Since image contrast in the nuclear medicine imaging is a measure of differences in the activity concentration in parts of the image corresponding to different levels of radioactive uptake in the patient, the accurate measurement of the image contrast is an important factor in estimation of the activity. Hence, we simulated a Siemens E.CAM SPECT system model with different commercial collimators using the SIMIND Monte Carlo program to study the effect of collimator choice and energy window width

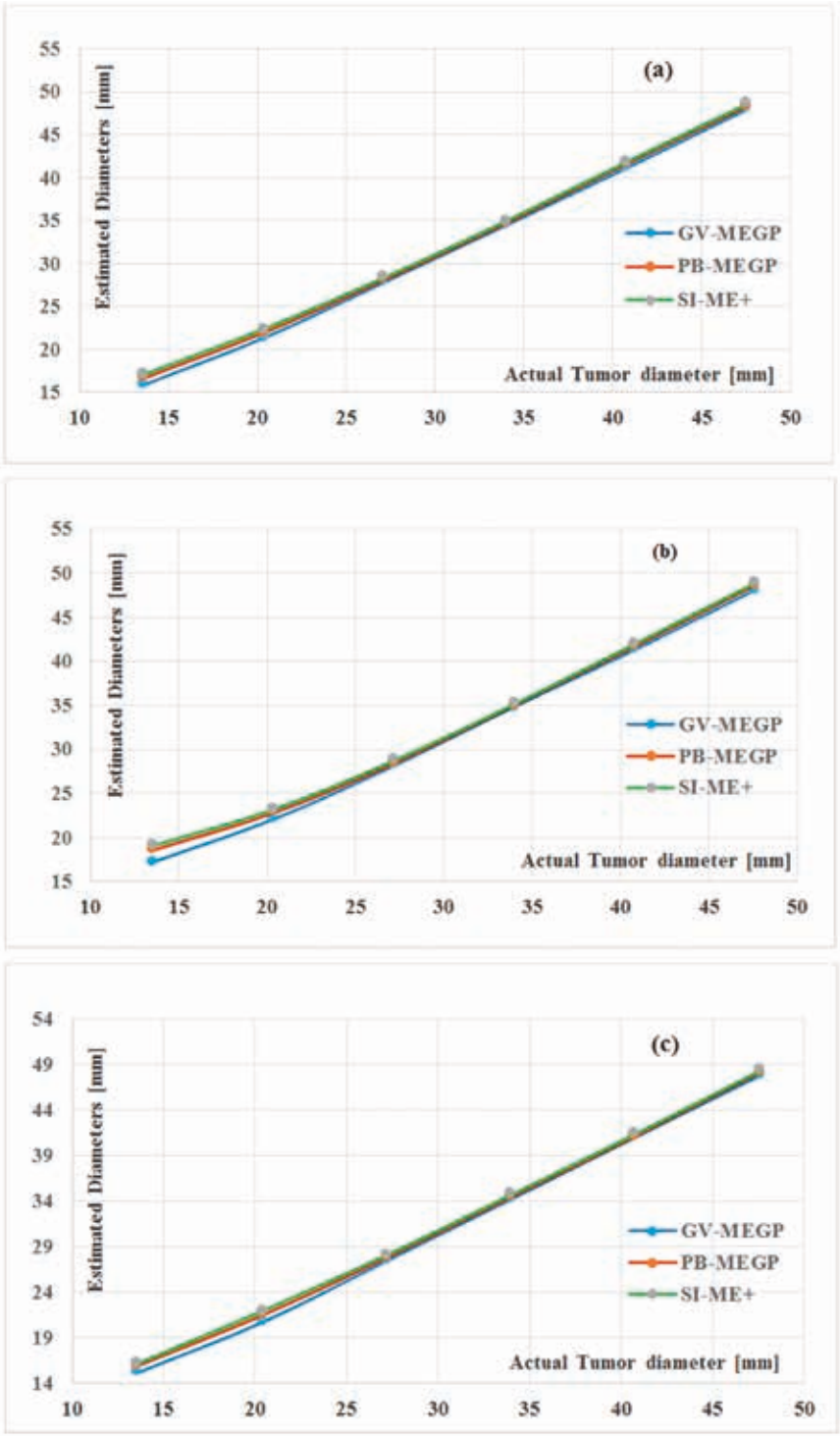

Figure 6. Estimated tumor diameters as a function of the actual liver tumor diameters in three different energy windows: (A) 60–160 keV, (B) 160–400 keV and (C) 60–400 keV using GV-MEGP, PB-MEGP, and SI-ME+ collimators

setting on the image contrast of Y-90 bremsstrahlung images of the liver tumors.

According to the results of the simulation for each collimator (Fig. 2 and Fig. 3), both the system sensitivity and image contrast were improved by use of the wide energy window ranging from 60 to 400 keV, which will lead to the decreased bias of the activity estimation [18]. Moreover, the system sensitivity and image contrast are also influenced by collimator geometry (i.e. hole diameter, collimator thickness and septal thickness). Although Roshan et al. [7] mentioned that image contrast can be increased by increasing the hole diameter and energy window width, for fixed collimator and septal thickness values for a specified collimator, our results indicated that the collimator thickness and septal thickness can also have significant effects on the image quality in the Y-90 bremsstrahlung SPECT imaging. For example, the PB-MEGP collimator has smaller hole diameter than PX-MEGP, but the evaluation of image quality of

the tumor showed that the PB-MEGP collimator produced better contrast. Thus, septal thickness and collimator thickness characteristics along with hole diameter were found to have a significant effect on the resulting image contrast in the bremsstrahlung SPECT imaging.

According to the performed simulations for liver tumors with various diameters, the choice of the collimator is very important for the assessment of small tumor sizes. For example, an accurate diagnosis of tumor size of 1.36 cm could not be made in the liver image acquired by the SPECT system equipped with the GE-HEGP collimator. Our results showed that the effect of collimator on the image quality is much more than energy window. For example, the contrast of tumor images acquired with the PB-MEGP collimator in the 1st energy window is better than the contrast acquired with the SE-HE collimator in the wide energy window, for each size of the tumor.

Our results showed ME collimators to be more appropriate for improving the imaging contrast of Y-90 bremsstrahlung photons than HE collimators. According to the results, the GV-MEGP collimator produced better results for the image contrast than the other parallel-hole collimators on all imaging performance (except for the system sensitivity), which has hole diameter, collimator thickness, and septal thickness: 0.3, 5.8, and 0.105 cm, respectively. The fraction of the septal penetration and sensitivity were achieved 0.81 % and 3.4824 cps/MBq, respectively, for GV-MEGP collimator, as listed in Table 2. In addition to, the optimal energy window was found ranging from 60 to 400 keV for all of the collimators. Y-90 bremsstrahlung SPECT images with a high contrast can improve the estimation of the Y-90 microsphere activity distribution after radiation therapy and treatment efficacy.

Our results indicated that the energy window and collimator geometry have also significant effects on the estimation of tumor size as quantitative assessment provided that microspheres accumulate in the tumor. The results indicated that the use of the GV-MEGP collimator could improve the estimation of tumor size by the FWHM method in the wide energy window, which will be useful in the assessment of liver tumor response to the therapy. The estimation of distribution sizes was close to the actual values for the tumor sizes with the diameters larger than 2.04 cm. Liver tumor size measured by FWHM method seems to be overestimated in tumors smaller than 2.04 cm, although each tumor included the same concentration of the Y-90 radionuclide. Nevertheless, it is important to mention that because of the shortened range of electrons in the tissue, tumor size is overestimated in all cases in the Y-90 bremsstrahlung SPECT imaging.

Conclusion

We investigated the effect of the commercial parallel hole collimators and energy window width on the image contrast of the Y-90 bremsstrahlung SPECT images of the liver tumors, as well as distribution size by using SIMIND Monte Carlo simulation program. According to the image contrast results, the collimator geometric parameters (i.e. hole diameter, septal thickness, and collimator thickness) are important factors in the bremsstrahlung imaging. We were able to identify the combination of energy window and collimator that was most suitable for improving Y-90 photon imaging in the human phantom. Our study showed that the GV-MEGP collimator and energy window width ranging from 60 to 400 keV can provide the best image contrast relative to the other energy windows and collimators in the Y-90 bremsstrahlung SPECT imaging of the liver tumors with different sizes. The high quality Y-90 bremsstrahlung images can provide reliable estimate of the Y-90 activity distribution after radiation therapy. Furthermore, we found the GV-MEGP collimator to be more appropriate for distribution size estimation, especially for tumor diameters larger than 2.04 cm, which is useful in assessing liver tumor response to the therapy. Although the microspheres distribution in the tumors and liver can change slightly in the clinical approach due to the patient body, the method presented in this paper may contribute toward obtaining better Y-90 bremsstrahlung images in the clinical study.

Acknowledgments

The authors would like to thank Professor Ljungberg for providing the valuable advices.

References

1. Ahmadzadehfar H, Biersack HJ, Ezziddin S. Radioembolization of liver tumors with yttrium-90 microspheres. Semin Nucl Med. 2010; 40(2): 105–121, doi: 10.1053/j.semnuclmed.2009.11.001, indexed in Pubmed: 20113679.
2. Rong X, Frey EC. A collimator optimization method for quantitative imaging: application to Y-90 bremsstrahlung SPECT. Med Phys. 2013; 40(8): 082504, doi: 10.1118/1.4813297, indexed in Pubmed: 23927349.
3. Minarik D, Sjögreen Gleisner K, Ljungberg M. Evaluation of quantitative (90)Y SPECT based on experimental phantom studies. Phys Med Biol. 2008; 53(20): 5689–5703, doi: 10.1088/0031-9155/53/20/008, indexed in Pubmed: 18812648.
4. Rong X, Du Y, Ljungberg M, et al. Development and evaluation of an improved quantitative (90)Y bremsstrahlung SPECT method. Med Phys. 2012; 39(5): 2346–2358, doi: 10.1118/1.3700174, indexed in Pubmed: 22559605.
5. Bonutti F, Avolio M, Magro G, et al. Optimization of the image contrast in SPECT-CT bremsstrahlung imaging for Selective Internal Radiation Therapy of liver malignancies with Y-90 microspheres. arXiv:1509.08857 [physics.med-ph]. 2015; 1–13. ArXiv:1509.08857.
6. Chery SR, Sorenson JA, Phelps ME. Physics in Nuclear Medicine. Elsevier/Saunders Philadelphia. 2012.
7. Roshan HR, Mahmoudian B, Gharepapagh E, et al. Collimator and energy window optimization for Y-90 bremsstrahlung SPECT imaging: A SIMIND Monte Carlo study. Appl Radiat Isot. 2016; 108: 124–128, doi: 10.1016/j.apradiso.2015.12.041, indexed in Pubmed: 26720261.
8. Walrand S, Hesse M, Wojcik R, et al. Optimal design of anger camera for bremsstrahlung imaging: monte carlo evaluation. Front Oncol. 2014; 4(149): 1–7, doi: 10.3389/fonc.2014.00149, indexed in Pubmed: 24982849.
9. Förnvik D, Zackrisson S, Ljungberg O, et al. Breast tomosynthesis: Accuracy of tumor measurement compared with digital mammography and ultrasonography. Acta Radiol. 2010; 51(3): 240–247, doi: 10.3109/02841850903524447, indexed in Pubmed: 20105090.
10. Rong X, Du Y, Frey EC. A method for energy window optimization for quantitative tasks that includes the effects of model-mismatch on bias: application to Y-90 bremsstrahlung SPECT imaging. Phys Med Biol. 2012; 57(12): 3711–3725, doi: 10.1088/0031-9155/57/12/3711, indexed in Pubmed: 22617760.
11. Roshan HR, Azarm A, Mahmoudian B, et al. Advances in SPECT for Optimizing the Liver Tumors Radioembolization Using Yttrium-90 Microspheres. World J Nucl Med. 2015; 14(2): 75–80, doi: 10.4103/1450-1147.157120, indexed in Pubmed: 26097416.

12. Gonzalez-Guindalini FD, Botelho MPF, Harmath CB, et al. Assessment of liver tumor response to therapy: role of quantitative imaging. Radiographics. 2013; 33(6): 1781–1800, doi: 10.1148/rg.336135511, indexed in Pubmed: 24108562.
13. Hruska CB, O'Connor MK. Quantification of lesion size, depth, and uptake using a dual-head molecular breast imaging system. Med Phys. 2008; 35(4): 1365–1376, doi: 10.1118/1.2885371, indexed in Pubmed: 18491531.
14. Tan YC, Chiu WK, Rajic N. Quantitative Defect Detection on the Underside of a Flat Plate Using Mobile Thermal Scanning. Procedia Engineering. 2017; 188: 493–498, doi: 10.1016/j.proeng.2017.04.513.
15. Ljungberg M. The SIMIND Monte Carlo program. Monte Carlo Calculations in Nuclear Medicine: Applications in Diagnostic Imaging. CRC Press, Boca Raton U.S.A. 2012.
16. DeWerd LA. The phantoms of medical and health physics. Kissick M (ed.), Springer 2014.
17. MATLAB. version 8.1 (R2013a). Natick, Massachusetts: The MathWorks Inc.; 2013.
18. Rong X, Ghaly M, Frey EC. Optimization of energy window for 90Y bremsstrahlung SPECT imaging for detection tasks using the ideal observer with model-mismatch. Med Phys. 2013; 40(6): 062502, doi: 10.1118/1.4805095, indexed in Pubmed: 23718607.